1997MNRAS.288.1060B

Mon. Not. R. Astron. Soc. **288,** 1060–1072 (1997)

Resolution requirements for smoothed particle hydrodynamics calculations with self-gravity

Matthew R. Bate and Andreas Burkert

Max-Planck-Institut für Astronomie, Königstuhl 17, D-69117 Heidelberg, Germany

Accepted 1997 March 14. Received 1997 February 28; in original form 1996 December 30

Downloaded from https://academic.oup.com/mnras/article/288/4/1060/974629 by guest on 20 August 2022

ABSTRACT

We determine a new resolution requirement for the smoothed particle hydrodynamics (SPH) numerical method when self-gravity is included. Comparison calculations between an SPH code and an Eulerian grid code are performed. The calculations are of a computationally demanding molecular cloud collapse and fragmentation problem. We demonstrate that the results given by the two different hydrodynamic methods are in good agreement, so long as the minimum resolvable mass in the SPH calculations is always less than the Jeans mass. If this criterion is not satisfied, SPH may give incorrect results, with the stability of near-Jeans-mass clumps depending on the details of how the SPH code is implemented rather than on physical processes. We give examples, from the literature, of problems that have been encountered in simulations of star, galaxy and cosmological-structure formation where this resolution requirement is ignored.

Key words: hydrodynamics – methods: numerical – binaries: close – stars: formation – galaxies: formation – large-scale structure of Universe.

1 INTRODUCTION

The smoothed particle hydrodynamics (SPH) numerical method was introduced by Lucy (1977) and Gingold & Monaghan (1977). The main advantages of SPH over grid-based finite-difference methods are that it is Lagrangian and that it does not require a computational grid. This makes SPH well suited to problems with large density contrasts (e.g., cloud collapse/fragmentation, stellar collisions, galaxy interactions), since computational effort is not wasted simulating the low-density regions. Also, recent SPH implementations (e.g. Evrard 1988; Hernquist & Katz 1989; Benz 1990; Monaghan 1992) use spatially and temporally varying smoothing lengths, so that the resolution increases automatically with increasing density; the complex multigrid and adaptive-grid schemes that are used for finite-difference methods are avoided.

Since the creation of SPH, various comparisons have been performed between it and other hydrodynamical methods. Many authors have performed shock tube and spherical collapse calculations (e.g. Woodward & Colella 1984; Evrard 1988; Hernquist & Katz 1989; Steinmetz & Müller 1993). Steinmetz & Müller showed that SPH and the PPM numerical method give excellent agreement on a demanding blast wave problem and a spherical collapse problem if enough particles are used; although SPH accurately reproduces the global behaviour of the problem with both high and low resolution, the smoothing out of shocks over several smoothing lengths becomes more severe as the resolution is decreased. Comparisons between SPH and other codes have also been done for specific problems. Durisen et al. (1986) modelled rapidly rotating polytropes to determine whether they would undergo fission to form binary systems with two finite-difference codes and an SPH code. Steinmetz & Müller compared SPH simulations of the passage of a star close to a black hole with the results from a flux-corrected-transport (FCT) finite-difference scheme. Davies et al. (1993) modelled stellar collisions with both SPH and PPM codes. In all three cases, good agreement was obtained between the results produced with SPH and those from the FCT, PPM and other finite-difference schemes. Indeed, Steinmetz & Müller concluded that for problems involving complicated geometries and highly dynamical behaviour, SPH is often a better choice than a grid-based code. Durisen et al. concluded that SPH required less computational effort to obtain results that were equivalent to those obtained from their finite-difference schemes.

One of the main applications of SPH has been in the field of star formation. Surprisingly, there have been very few comparisons between SPH and other hydrodynamical

© 1997 RAS

© Royal Astronomical Society • Provided by the NASA Astrophysics Data System

1997MNRAS.288.1060B

methods for collapse and fragmentation problems. However, early in the development of SPH, a series of papers were produced on the 'standard isothermal test case' (Boss & Bodenheimer 1979) for the collapse and fragmentation of a molecular cloud core. In these papers, the results from SPH (Gingold & Monaghan 1981, 1982; Monaghan & Lattanzio 1985, 1986) and Eulerian grid codes (Boss & Bodenheimer 1979; Bodenheimer & Boss 1981) were compared. The SPH calculations disagreed with the finite-difference results. The finite-difference calculations produced two compact fragments whose density increased rapidly after their formation. Although the fragments could not be followed long enough to determine if they merged or formed a binary system, from their rate of collapse and their trajectories, Bodenheimer & Boss predicted that the fragments would not merge but would form a binary system. The SPH results, on the other hand, could be followed much longer than the finite-difference results because the binary fragments did not collapse quickly; only a slow contraction was observed. As the fragments fell towards each other, they were found to merge. The source of the disagreement was the large smoothing length used in the SPH calculations. When the size of the fragments became similar to the smoothing length, their collapse was artificially slowed, in the SPH calculations, because the gravitational forces were softened (see Section 3). Thus, when the fragments approached each other on highly elliptical orbits, their sizes were unphysically large, leading to a merger. Most recently, modern SPH (Bate, Bonnell & Price 1995) and Eulerian grid codes (Burkert & Bodenheimer 1993; Myhill & Boss 1993) have been shown to give excellent agreement on the standard test case, due to the use of spatially and temporally variable smoothing lengths in SPH. This allows the resolution to increase with the local density and, thus, a fragment to keep collapsing indefinitely to arbitrary densities. In agreement with the grid code, the new SPH calculations lead to the formation of compact fragments which do not merge artificially, but instead form a wide, elliptical binary system (Bate et al. 1995).

Although increased resolution eliminates the disagreement between SPH and other numerical methods on the 'standard isothermal test case', as with grid codes, there is always the question of 'How much resolution is enough?' The resolution required to resolve shocks and other purely hydrodynamic behaviour with SPH has been thoroughly explored (e.g. Monaghan 1992 and references within). However, the resolution that is required when SPH is combined with self-gravity still requires more investigation. It would be desirable to find a criterion for simulations of self-gravitating systems which determines the resolution that SPH requires in order to give the correct results. This is important not only for fragmentation calculations, but for any self-gravitating system that is simulated with SPH (e.g., cosmological-structure and galaxy formation).

In this paper, we show that SPH produces the correct results in problems involving self-gravity, so long as the minimum resolvable mass is always less than a Jeans mass. An equivalent statement is that the hydrodynamic smoothing length and gravitational softening length must always be less than the local Jeans length. This criterion is related to the problem that caused the early disagreement between finite-difference and SPH methods on the 'standard isothermal test case'. As an example of the resolution problem, we compare SPH with an Eulerian grid code on the difficult collapse/fragmentation problem that was first presented by Burkert & Bodenheimer (1993).

In Section 2, we briefly describe the implementations of the Eulerian and SPH codes. This is followed, in Section 3, by a discussion of the softening of gravitational forces in SPH, and examples of the unphysical effects that can be caused by the lack of resolution in fragmentation and galaxy formation calculations. Section 4 gives the initial conditions for the comparison calculation. The results from the Eulerian code are presented in Section 5. The SPH results for the initial fragmentation of the cloud into a binary are given in Section 6. These results are discussed in Section 7. In Section 8, we consider the fragmentation of the bar of gas between the binary fragments using SPH. Finally, in Section 9, we present our conclusions.

2 COMPUTATIONAL METHODS

2.1 Eulerian grid code

The hydrodynamical equations are integrated using a second-order finite-difference method as described by Burkert & Bodenheimer (1993, 1996). The calculations are performed on a three-dimensional Eulerian, Cartesian grid. The full computational region is represented by a standard grid with 64^3 grid cells, equally spaced in all directions. In order to improve the resolution in the inner regions, where fragmentation occurs, four Cartesian nested concentric subgrids, each with $128 \times 128 \times 64$ grid cells, are superimposed on the standard grid. The linear scale on the first subgrid is reduced by a factor of 4 with respect to the standard grid, and by additional factors of 2 for each subsequent subgrid, giving a ratio of cell size on the standard grid to smallest zone size of 32. The grid structure is set up at the beginning of the calculations and is left fixed during the entire run. Shocks are treated using an artificial viscosity of the type described by von Neumann & Richtmyer (1950). The dimensionless viscosity parameter is set to 0.1. We use an isothermal equation of state

$$P = c_s^2 \rho, \tag{1}$$

where P is the pressure, ρ is the density, and c_s is the sound speed of the gas. However, in order to prevent numerical fragmentation (Truelove et al. 1997), zones with exceptionally high densities are heated artificially to keep the local Jeans length larger than the zone size (Burkert, Bate & Bodenheimer 1997). The artificial heating coefficient η_ρ is taken to be 0.5.

2.2 SPH code

The SPH calculations were performed using a three-dimensional SPH code based on a version originally developed by Benz (Benz 1990; Benz et al. 1990). The code uses a tree to calculate gravitational forces and to find the nearest neighbours. The smoothing lengths of particles can vary in time and space, and do so to keep the number of neighbours approximately constant. A particle has $N_{\rm neigh} = 50$ neighbours on average. The standard form of artificial viscosity is used (Monaghan & Gingold 1983; Benz 1990; Monaghan

Downloaded from https://academic.oup.com/mnras/article/288/4/1060/974629 by guest on 20 August 2022

© Royal Astronomical Society • Provided by the NASA Astrophysics Data System

1997MNRAS.288.1060B

1992), with the parameters $\alpha_v = 1$ and $\beta_v = 2$. The SPH equations are integrated using a second-order Runge–Kutta–Fehlberg integrator. Individual time-steps are used for each particle (Bate et al. 1995).

Again, we use the isothermal equation of state given by equation (1) (with the exception of Section 8). However, if a pure isothermal equation of state is used, and if the smoothing lengths of particles are able to decrease without limit as the density increases, the SPH calculations cannot be followed after the first fragment forms because of the high particle densities (and therefore short time-steps) in the fragment. To avoid this, we introduce a minimum particle smoothing length (e.g. Bonnell et al. 1991). This slows the collapse of a fragment by reducing the gravitational forces between the particles in the fragment (see Section 3). Furthermore, if the fragment is rotating, its collapse will be stopped entirely when centrifugal forces become comparable to the reduced gravitational forces. Thus the simulation can be continued at the expense of ignoring the internal evolution of the fragment (e.g. Bonnell et al. 1991; Bate et al. 1995).

3 GRAVITATIONAL FORCES IN SPH

For the conclusions reached in this paper, it is important that we discuss the softening of gravitational forces that is used in SPH. Just as with an N-body code, the problem of a diverging gravitational force between two particles with small separations must be avoided. Two methods are commonly used. The first method (e.g. Evrard 1988) is to use the Plummer force law

$$F \propto r/(r^2+\epsilon^2)^{3/2} \tag{2}$$

that is commonly used in N-body codes. The smallest possible value of ϵ is determined by the requirement that the calculations are not dominated by particle–particle encounters. This force law is also used for implementations of SPH which use the special purpose GRAvity-PipE (GRAPE) hardware to calculate gravity forces and nearest neighbours (Steinmetz 1996). The second method is to soften gravitational forces using the SPH kernel (Gingold & Monaghan 1977; Hernquist & Katz 1989; Benz 1990). In SPH, the mass of a particle can be thought of as being smoothed out over the volume of the kernel, with the kernel function describing the particle's density distribution as a function of radius. We use the standard spline kernel (Monaghan & Lattanzio 1985)

$$W(r,\lambda) = \frac{1}{\pi\lambda^3} \begin{cases} 1-\frac{3}{2}q^2+\frac{3}{4}q^3 & \text{if } 0 \le q < 1 \\ \frac{1}{4}(2-q)^3 & \text{if } 1 \le q < 2 \\ 0 & \text{otherwise,} \end{cases} \tag{3}$$

where $q = r/\lambda$, r is the distance from the particle, and λ determines the width of the kernel. For hydrodynamic quantities, the parameter λ is known as the smoothing length and is given the symbol h. Using the interpretation that the density distribution of a particle is smoothed out over a kernel, when two particles approach each other, the gravitational force between them is naturally softened, with the gravitational softening length $\epsilon = \lambda = h$ (e.g. Benz 1990).

The kernel method has the advantage that, for the kernel of equation (3), the gravity is Newtonian outside 2ϵ, whereas the Plummer force law only converges slowly to the Newtonian value. Also, using kernel softening is the more natural method, since the concept of a particle's mass being smoothed out over the volume of the kernel gives both the hydrodynamic and gravitational forces. Note, however, that the kernel method for softening gravity may also be used with a value of ϵ that is *independent* of h (e.g. Hernquist & Katz 1989). One reason to do so is because, if $\epsilon = h$ and variable smoothing lengths are used, the potential energy of a particle is continuously changing. However, these changes can easily be accounted for when calculating the potential energy of the system (Benz 1990), and the advantage of having $\epsilon = h$ is that the gravity and hydrodynamic resolutions are equal.

If the gravitational softening length ϵ is kept fixed, and yet variable hydrodynamic smoothing lengths are used, ϵ and h may become very different from each other. We now investigate the effect this has on an SPH calculation. Consider a marginally stable, Jeans-mass clump of gas with mass M_J and radius R_J. For the clump to be stable against gravitational collapse, the outwards pressure force on a particle has to balance the inwards gravitational force. If R_J is much larger than h and ϵ, the SPH forces are good approximations to the true forces. However, if R_J is similar to h, the pressure forces are smoothed, and if R_J is similar to ϵ, the gravitational forces are softened. Thus the behaviour of such a clump depends on the method by which the smoothing and softening are performed.

Consider two SPH particles in a Jeans-mass clump of gas with $R_J \approx h$. The forces between them, as a function of separation, are plotted in Fig. 1(a). If $\epsilon = h$, the ratio of the gravitational to the pressure forces between them is approximately equal to unity and is roughly constant for $r < h$ (Fig. 1b, medium-thickness lines). However, if $\epsilon > h$, pressure forces dominate over gravitational forces (Fig. 1b, thin lines), while, if $\epsilon < h$, gravitational forces dominate over pressure forces (Fig. 1b, thick lines). Moreover, these effects increase as the separation between the particles is decreased. For a clump that is very stable against collapse or a clump that is massively unstable this makes little difference. However, if $M \approx M_J$ (i.e., the clump is self-gravitating) the details of how the softening and smoothing are done determine whether the clump is stable or unstable to collapse. If $\epsilon > h$, pressure forces dominate over gravity forces and the clump will try to expand; a marginally Jeans-unstable clump is *stabilized* against collapse. If $\epsilon < h$, artificial collapse on a scale smaller than the formal resolution of SPH may be induced *inside* a marginally Jeans-stable clump (see Section 7), since gravitational forces between particles within a subclump may strongly dominate over pressure forces, and this domination increases as the particles contract towards each other. Finally, note that with $\epsilon = h$, a Jeans-unstable clump will collapse; however, its collapse will be *slower* than is physical, since both the pressure forces and gravitational forces within the clump are reduced in magnitude.

In summary, if a clump of gas with $M \approx M_J$ has a radius close to h or ϵ, the SPH code has reached its resolution limit. Going beyond this limit may lead to unphysical results, since the stability of the clump against collapse depends on the

Downloaded from https://academic.oup.com/mnras/article/288/4/1060/974629 by guest on 20 August 2022

© Royal Astronomical Society • Provided by the NASA Astrophysics Data System

1997MNRAS.288.1060B

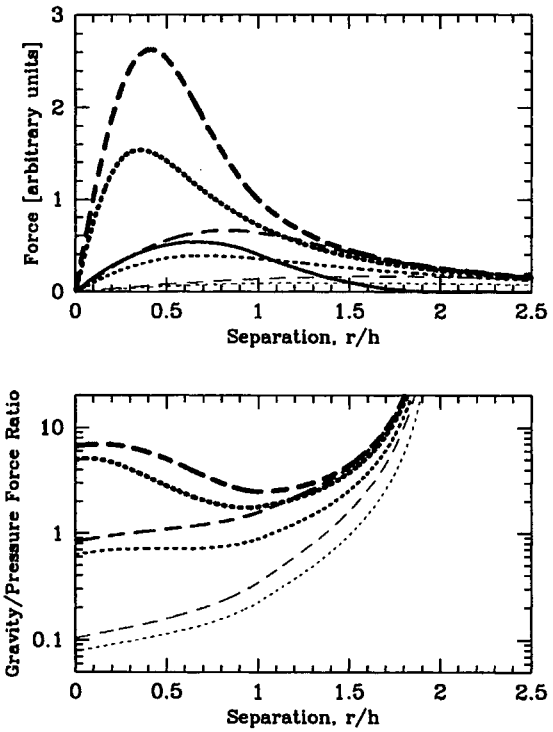

Figure 1. In the upper graph (a), the pressure forces (solid line) and gravitational forces between two particles within a Jeans-mass clump of radius $R=h$ are given as a function of the separation r of the particles. Gravitational forces are given using the Plummer force law (dotted) and kernel softening (dashed) with the gravity softening length ϵ equal to the hydrodynamic smoothing length h (medium-thickness lines), with $\epsilon=h/2$ (thick lines), and with $\epsilon=2h$ (thin lines). In the lower graph (b), the ratios of the various forms of gravitational force to the pressure force are given. Note that, if $\epsilon<h$, gravity dominates over pressure while, when $\epsilon>h$, pressure forces dominate over gravitational forces for separations $r\lesssim 1.5h$.

gravitational force law and the kernel functions that are used (which may differ from those described above), rather than on physical processes. In the following section, we give examples from the literature of how exceeding this limit may affect SPH calculations.

3.1 Examples of the unphysical effects of SPH gravity softening

3.1.1 Fragmentation calculations

If an SPH code is implemented so that $\epsilon=h$ and a minimum smoothing length is enforced, gravitational forces on scales less than ϵ are reduced *regardless* of the number of particles within a kernel. This can be helpful. For example, such a method slows the collapse of high-density fragments when their size is close to minimum smoothing length and, thus, allows fragmentation calculations to be continued much longer than if the fragments were allowed to collapse freely (as described in Section 2.2).

However, the reduction of gravitational forces on scales less than ϵ is also responsible for the early disagreement between SPH and finite-difference methods on the 'standard isothermal test case' (see Section 1). Fig. 2 gives

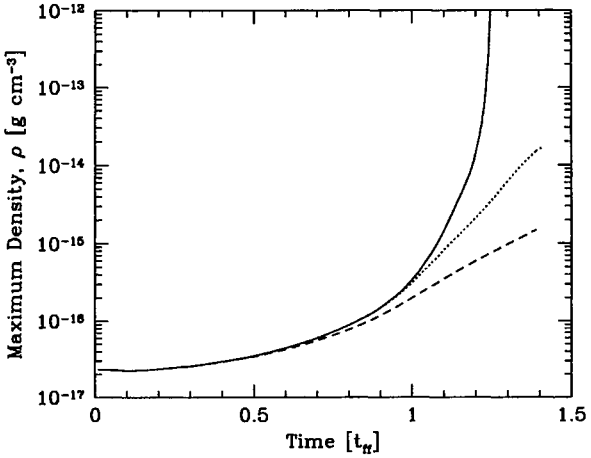

Figure 2. The maximum density versus time for the 'standard isothermal test case' (Boss & Bodenheimer 1979). The calculations were performed using SPH with the gravitational softening length equal to the hydrodynamic smoothing length $\epsilon=h$ and with no minimum smoothing length (solid line) or minimum smoothing lengths of 5 per cent (dotted line) and 10 per cent (dashed line) of the initial cloud radius. Time is given in units of the initial cloud free-fall time $t_{\rm ff}=5.52\times10^{11}$ s. The calculation was performed with 8.0×10^3 particles.

the maximum density versus time for three calculations of the 'standard isothermal test case'. The calculations were performed using SPH with $\epsilon=h$ and kernel softening. They are similar to those presented by Bate et al. (1995). The three calculations are identical to each other, except in their use of a minimum smoothing length. In one calculation, no minimum smoothing length is used, while the other two use minimum smoothing lengths of 5 and 10 per cent of the initial cloud radius. It is observed that while the calculation with no minimum smoothing length (Fig. 2, solid line) collapses rapidly towards infinite density at $t\approx1.26\,t_{\rm ff}$, the calculations with the minimum smoothing lengths (Fig. 2, dotted and dashed lines) show only a slow contraction of the fragments because of the softening of gravitational forces between particles with a kernel. Although early SPH calculations did allow for the smoothing lengths to decrease as the cloud collapsed, the smoothing lengths were still large because a global (rather than local) smoothing length was used for all particles. For example, in the calculation of the 'standard isothermal test case', performed by Gingold & Monaghan (1981), the smoothing lengths began at 10 per cent of the initial cloud radius and were reduced to a minimum of 3 per cent during the calculation. The use of large smoothing lengths is not crucial when the gas within a kernel has less than a Jeans mass, since then it cannot collapse under its own gravity. However, when the mass of the gas contained within a kernel becomes greater than a Jeans mass, its collapse is inhibited by the softening of the gravitational forces; it only contracts slowly rather than collapsing on a free-fall time-scale. When the 'standard isothermal test case' was performed with early SPH codes and the results compared to a finite-difference code, this unphysically slow contraction of two fragments as they fell towards each other resulted in their merger (with SPH) rather than the formation of a binary system (with a finite-difference code). The

© Royal Astronomical Society • Provided by the NASA Astrophysics Data System

Downloaded from https://academic.oup.com/mnras/article/288/4/1060/974629 by guest on 20 August 2022

1997MNRAS.288.1060B

use of a spatially and temporally variable smoothing length in modern SPH codes helps alleviate this problem. However, as we demonstrate in the following sections, a problem can still occur because an SPH kernel is still constrained to contain a fixed number of particles, and the combined mass of these particles may exceed a Jeans mass.

As hinted at above, in SPH implementations where ϵ and h are not constrained to be equal, the numerical effects on a fragmentation calculation may be even more important. If $\epsilon > h$, Jeans-unstable clumps on the scale of ϵ will be stabilized against collapse. If $\epsilon < h$, artificial collapse of Jeans-stable clumps on the scale of h may be induced, as will be demonstrated in Section 7.

3.1.2 Cosmological-structure and galaxy formation calculations

The effects of gravity softening in SPH are not limited to molecular cloud fragmentation calculations. Whenever self-gravitating gaseous clumps are formed, the question of resolution must be addressed. Sommer-Larsen, Vedel & Hellsten (1997) considered the effects of hydrodynamic smoothing and gravity softening on calculations of galaxy formation. They showed that, if $\epsilon > h$, then unphysical, self-gravitating, isothermal, stationary gas spheres may be formed as a consequence of the softened gravitational forces; as described above, if $\epsilon > h$, softening of gravity leads to Jeans-unstable clumps being stabilized against collapse. They concluded that care should be taken when comparing the results from such calculations to reality.

Owen & Villumsen (1997) performed two-dimensional calculations of cosmological-structure formation using an SPH code with baryonic and dark matter. They found that as they increased the resolution of their calculations, the dark matter results converged, but the baryonic matter results did not. With the dark matter, although the structure became more clearly defined with higher resolution, the underlying particle distribution was the same. However, the baryons were found to be systematically more collapsed with increased resolution. To achieve convergence of the baryonic matter, Owen & Villumsen had to introduce a minimum temperature and, hence, minimum Jeans mass. Once this minimum Jeans mass was resolved, the baryonic matter results converged with increasing resolution. They attributed this dependence of the degree of collapse of the baryons to differences in the resolution of shocks. However, it is likely that this dependence of the degree of collapse is instead due to the unphysical behaviour of unresolved Jeans-unstable clumps that we describe here.

4 THE COMPARISON CALCULATION

As the comparison calculation to demonstrate the unphysical behaviour that can be caused by insufficient resolution in self-gravitating SPH calculations, we use the computationally demanding fragmentation calculation that was recently presented by Burkert & Bodenheimer (1993). The initial conditions for the cloud are similar to those of the 'standard isothermal test case' (Boss & Bodenheimer 1979), the main difference being the smaller non-axisymmetric density perturbation. The initial cloud is a sphere of radius $R = 5 \times 10^{16}$ cm and mass $M = 1\ \mathrm{M}_{\odot}$ in uniform rotation with an angular velocity of $\Omega = 7.2 \times 10^{-13}$ rad s^{-1}. The cloud has an underlying constant density with a non-axisymmetric $m = 2$ perturbation of 10 per cent amplitude

$$\rho = \rho_0[1 + 0.1\cos(2\phi)], \tag{4}$$

where ϕ is the azimuthal angle about the rotation (z) axis and $\rho_0 = 3.82 \times 10^{-18}$ g cm^{-3}. The sound speed of the gas is $c_s = 1.66 \times 10^4$ cm s^{-1}. The ratios of the thermal and rotational energies to the magnitude of the gravitational potential energy are $\alpha = 0.26$ and $\beta = 0.16$, respectively.

This collapse/fragmentation problem is demanding, because the fragmentation occurs only in the very central regions of the cloud. Thus, for a grid code, multiply nested subgrids have to be used in order to achieve the required resolution. SPH does not have spatially limited resolution like a grid code if the smoothing lengths of particles decrease as the density increases. However, this calculation is also demanding for SPH because of the low mass fraction that is contained in the volume where the fragments form; a large total number of particles are required because only a small fraction of them are contained in the central region where the fragmentation occurs.

5 EULERIAN GRID-CODE RESULTS

In Fig. 3 we give the density and velocity of the gas during the collapse and fragmentation of the molecular cloud core using the Eulerian grid code. The initial evolution is as presented in (Burkert & Bodenheimer 1993).

In the early stages of evolution the initial density perturbation causes an expansion in the central parts of the cloud. An inner region of almost constant density is established with two overdense zones at the outer edge of the rarefaction wave which result from the initial $m = 2$ perturbation. After one free-fall time, $t_{\mathrm{ff}} = 1.0774 \times 10^{12}$ s, this region starts to collapse again and forms an elongated high-density structure. Due to the converging flow, gas from the infalling envelope accumulates fastest at the two ends of this bar. The ends become self-gravitating, collapse on to themselves and form two condensed fragments. Mass continues to flow into the region between the binary fragments, leading to the formation of a connecting high-density bar which subsequently fragments too.

6 SPH BINARY FRAGMENTATION AND BAR FORMATION

We now present the results obtained using SPH. Calculations were performed using 1.0×10^4, 2.0×10^4, 3.0×10^4, 4.0×10^4 and 8.0×10^4 particles. We use the isothermal equation of state. To stop the collapse of fragments to infinite densities, which would require the calculations to be stopped when the first fragment forms, we use a minimum particle smoothing length of 10^{14} cm. This gives the minimum spatial resolution of the SPH calculations which is almost two orders of magnitude smaller than the separation of the binary that forms with the finite-difference code. Hence the use of the minimum smoothing length cannot affect the formation of the binary or cause it to merge artificially. Unless otherwise stated, we use the kernel to soften the gravitational forces and $\epsilon = h$.

Downloaded from https://academic.oup.com/mnras/article/288/4/1060/974629 by guest on 20 August 2022

© Royal Astronomical Society • Provided by the NASA Astrophysics Data System

1997MNRAS.288.1060B

The fragmentation of the cloud can be divided into two main parts: (a) the fragmentation of the cloud into a binary and the formation of a bar between the two fragments; and (b) the growth of the bar in mass, and its subsequent fragmentation into multiple fragments. Each stage is investigated separately. In this section, we concentrate on the binary fragmentation and bar formation. The problem of the bar fragmentation is left to Section 8.

6.1 High-resolution SPH

Good agreement is obtained between the grid code and the highest resolution SPH calculation, with 8.0×10^4 particles (cf. Figs 3 and 4). All the major qualitative phases that were present in the grid-code calculations are also found in the high-resolution SPH calculation. Initially, the centre of the cloud expands. The expansion sweeps up material and causes two overdense regions to be formed from the initial $m=2$ perturbation. When the cloud begins to collapse again, the two overdense regions fall towards the centre of the cloud (Fig. 4 at $t=1.00\,t_{\rm ff}$), and merge to form a prolate, elongated structure (Fig. 4 at $t=1.15\,t_{\rm ff}$). As more material falls on to the elongated structure, the ends become self-gravitating (at $t\approx1.20\,t_{\rm ff}$) and collapse upon themselves to form two protostellar fragments (Fig. 4 at $t=1.26\,t_{\rm ff}$). Between these two fragments is a low-density bar. This bar increases in density due to material flowing into it (Fig. 4 at $t=1.26$–$1.29\,t_{\rm ff}$). When the density along the bar becomes approximately uniform, it fragments into many pieces (see Section 8).

The maximum and central densities as functions of time are compared to those from the grid code in Fig. 5. Both codes give similar behaviour, with two minor differences. The density peak that is given by the grid code at $t\approx1.12\,t_{\rm ff}$ is not given by the SPH code, because the resolution of the SPH code is lower when the two overdense regions merge. Also, the times at which the fragments are formed differs slightly between the codes, with the SPH code taking $\approx0.02\,t_{\rm ff}$ longer. Note that, with both the grid code and the SPH code, the maximum density increases only slowly and the central density is stable from $t=1.15$ to $1.20\,t_{\rm ff}$. This is the period during which the elongated structure (formed from the merger of the two overdense regions) is growing in mass. The two codes give excellent agreement in the central density during this quasi-static phase. Once the two ends of the structure each contain roughly a Jeans mass (at $t\approx1.20\,t_{\rm ff}$), they collapse more or less independently to form the binary.

6.2 Low-resolution SPH

With low resolution (Fig. 6), using only 1.0×10^4 particles, the grid code and SPH show good agreement only up until $t\approx1.10\,t_{\rm ff}$. The initial expansion in the central regions of the cloud is reproduced with 1.0×10^4 particles, as is the formation of two overdense regions at the edge of the cloud's core and their merger to form an elongated structure (Fig. 6 at $t=1.00$–$1.15\,t_{\rm ff}$). However, as the elongated structure increases in mass, it collapses to form a bar, rather than

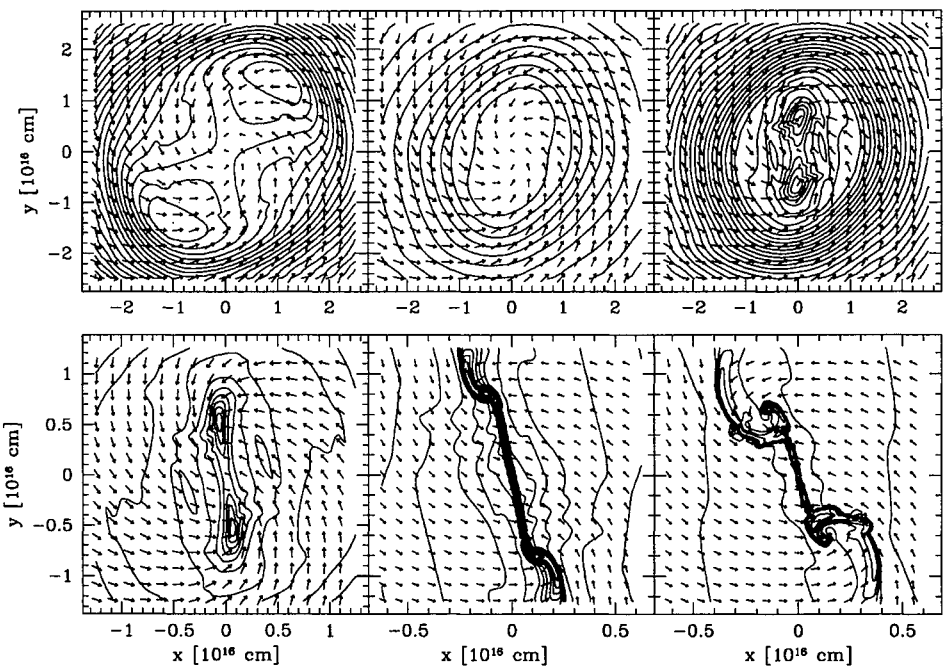

Figure 3. Density and velocity in the x–y plane for the binary-bar fragmentation test calculation performed with a grid code. Contours of equal density are shown. Velocity arrows give the direction of the flow with the length of an arrow proportional to the speed. The time t in units of the initial cloud free-fall time $t_{\rm ff}=1.0774\times10^{12}$ s, contour interval $\Delta\log\rho$ and the maximum velocity $v_{\rm max}$ are: (upper left panel) $t=1.0\,t_{\rm ff}$, $\Delta\log\rho=0.05$, $v_{\rm max}=4.79\times10^4$ cm s^{-1}; (upper middle panel) $t=1.1\,t_{\rm ff}$, $\Delta\log\rho=0.25$, $v_{\rm max}=5.43\times10^4$ cm s^{-1}; (upper right panel) $t=1.15\,t_{\rm ff}$, $\Delta\log\rho=0.10$, $v_{\rm max}=6.01\times10^4$ cm s^{-1}; (lower left panel) $t=1.23\,t_{\rm ff}$, $\Delta\log\rho=0.25$, $v_{\rm max}=8.58\times10^4$ cm s^{-1}; (lower middle panel) $t=1.26\,t_{\rm ff}$, $\Delta\log\rho=0.25$, $v_{\rm max}=14.40\times10^4$ cm s^{-1}; (lower right panel) $t=1.29\,t_{\rm ff}$, $\Delta\log\rho=0.50$, $v_{\rm max}=18.69\times10^4$ cm s^{-1}.

© Royal Astronomical Society • Provided by the NASA Astrophysics Data System

Downloaded from https://academic.oup.com/mnras/article/288/4/1060/974629 by guest on 20 August 2022

1997MNRAS.288.1060B

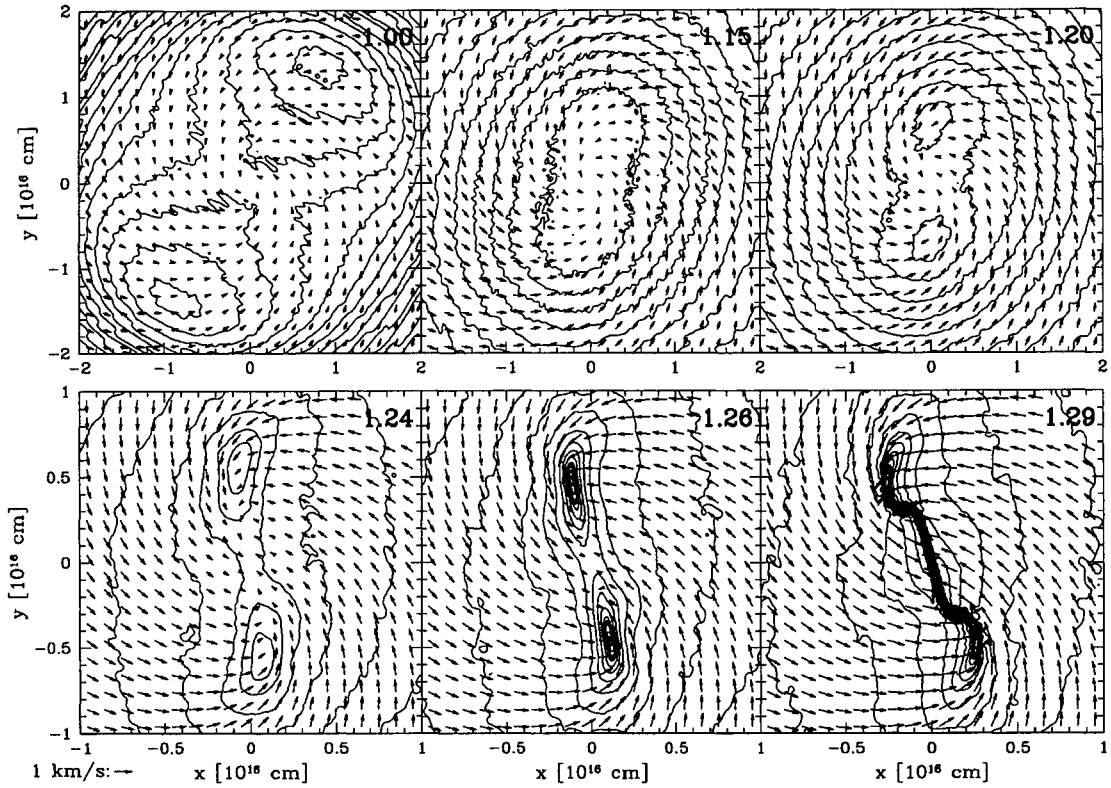

Figure 4. Density and velocity in the x–y plane for the binary-bar fragmentation test calculation performed with SPH using 8.0×10^4 particles. Density contours are drawn every 1/20 of a decade in the first frame, and 1/4 of a decade in the other frames. In addition, the heavy-density contour shows the region within which $\rho > \rho_{\rm crit}$. Velocity vectors are given with length proportional to speed; an arrow representing 1 km s^{-1} is given beneath the frames. Times are given for each frame in units of the initial cloud free-fall time $t_{\rm ff} = 1.0774 \times 10^{12}$ s.

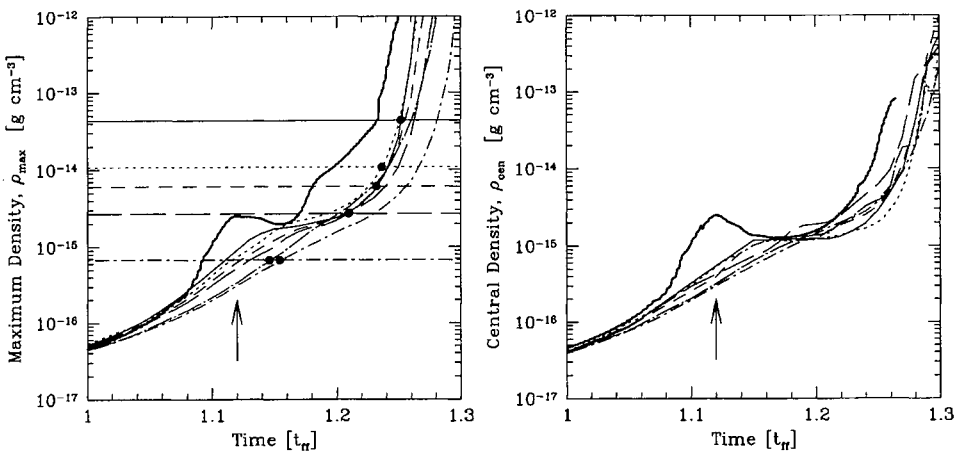

Figure 5. Maximum density $\rho_{\rm max}$ (left) and the density in the centre of the coordinate system $\rho_{\rm cen}$ (right) versus time. Results from the Eulerian grid code are given (thick solid lines), along with those from SPH calculations performed with 8.0×10^4 (solid lines), 4.0×10^4 (dotted lines), 3.0×10^4 (dashed lines), 2.0×10^4 (long-dashed lines), and 1.0×10^4 (dot–dashed lines) particles. There are two 1.0×10^4 particle simulations, one performed with $\epsilon = h$ (dot–short-dashed lines), and one with $\epsilon = 1.0 \times 10^{14}$ cm (dot–long-dashed lines). The horizontal lines give the critical density $\rho_{\rm crit}$ below which a Jeans mass is resolved in each SPH calculation. The filled dots give the points at which each calculation surpasses $\rho_{\rm crit}$. The arrows indicate the time at which the elongated structure is formed by the merger of the two overdense regions in the grid-code calculation. The free-fall time is $t_{\rm ff} = 1.0774 \times 10^{12}$ s.

forming two independent self-gravitating cores (Fig. 6 at $t = 1.20\,t_{\rm ff}$). The collapse of the bar continues, primarily along its minor axes, to form a high-density spindle (Fig. 6 at $t = 1.24$–$1.29\,t_{\rm ff}$). Eventually, the spindle forms multiple fragments.

6.3 Medium-resolution SPH

With intermediate resolutions of 2.0×10^4, 3.0×10^4 and 4.0×10^4 particles, the fragmentation proceeds as in the high-resolution calculation (e.g. Fig. 7): two equal-mass

© Royal Astronomical Society • Provided by the NASA Astrophysics Data System

Downloaded from https://academic.oup.com/mnras/article/288/4/1060/974629 by guest on 20 August 2022

1997MNRAS.288.1060B

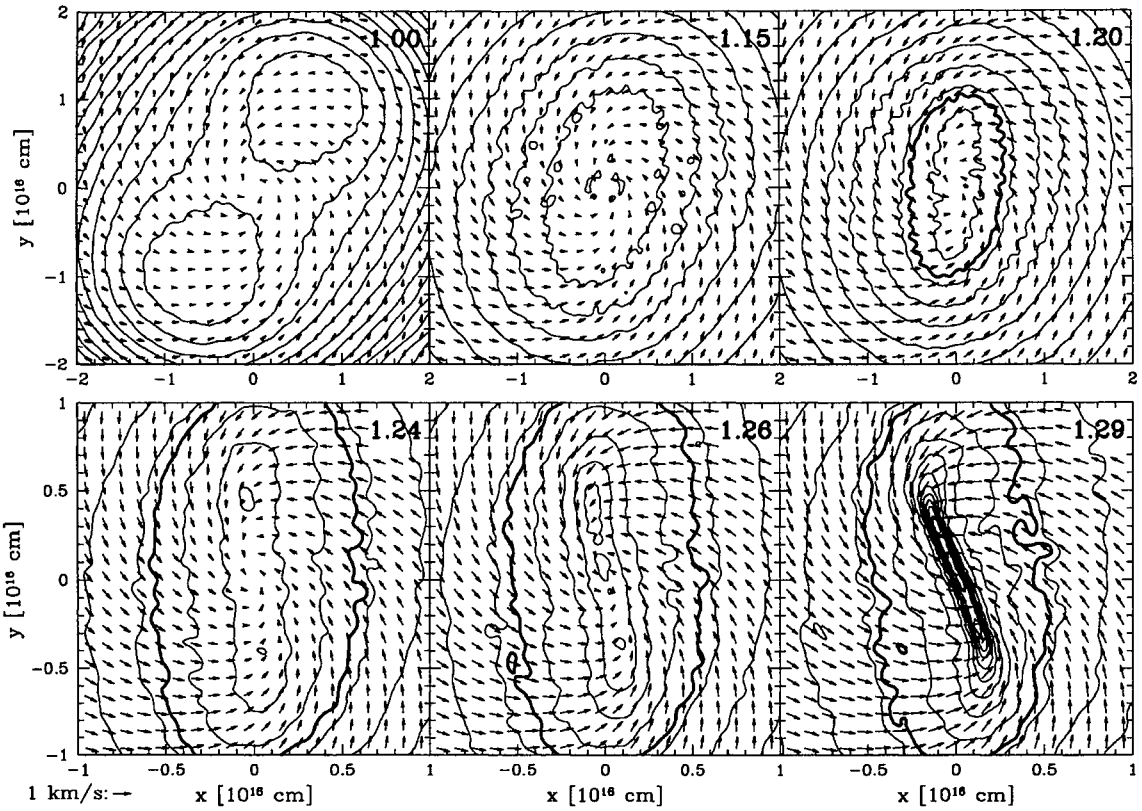

Figure 6. Density and velocity in the x–y plane for the binary-bar fragmentation test calculation performed with SPH using 1.0×10^4 particles. See Fig. 4 for details.

fragments form with a low-density bar of gas between them; the bar increases in density via accretion and eventually fragments. However, with these resolutions, the difference in density between the bar and the fragments is less pronounced than for the highest resolution calculation (cf. Figs 4 and 7) due to greater smoothing. The resolution is only just high enough with 2.0×10^4 particles to resolve the binary fragmentation. Calculations performed with 3.0×10^4 and 4.0×10^4 particles quickly converge to the result given with 8.0×10^4 particles, with a much greater distinction between the bar and the fragments than with only 2.0×10^4 particles.

7 DISCUSSION OF THE BINARY FRAGMENTATION

If SPH is implemented with spatially and temporally variable smoothing and softening lengths then, unlike a grid-based code, there is no fixed spatial limit on its resolution (unless a minimum smoothing length is introduced). However, although there is no fixed *spatial* resolution limit, there is a fixed *mass* resolution limit. The variable smoothing lengths of particles are constrained to contain a roughly constant number of particles ($N_{\rm neigh} = 50$) and, hence, a certain mass (assuming that all particles are of equal mass). Therefore SPH has *mass-limited resolution*. For a clump of gas to be resolved, its behaviour must be dominated by physical processes, and not the numerical implementation. As described in Section 3, the behaviour of a Jeans-mass clump of gas with radius $\approx h$ is dominated by the numerical implementation. Thus the minimum resolvable mass must be significantly larger than the number of particles contained within a volume of radius h. Navarro & White (1993) (using $N_{\rm neigh} = 40$) found that $\gtrsim 100$ particles were required to give reasonable results when modelling the adiabatic collapse and virialization of a gas cloud or modelling the merging of two clumps of gas. Thus we take the smallest mass that an SPH calculation can resolve to be equal to the mass of $\approx 2N_{\rm neigh}$ particles. Note also that this resolution limit can be expressed as a spatial resolution limit, since $2N_{\rm neigh}$ particles are contained within sphere of radius $\approx 3h$. This resolution limit does not affect the global results of an SPH fragmentation calculation unless the Jeans mass becomes comparable to the mass of $2N_{\rm neigh}$ particles (or, alternately, the Jeans radius becomes comparable to $\approx 3h$). In this case, the stability of the clump against collapse depends on the details of how the gravitational forces are softened and the pressure forces are smoothed (Section 3). In the calculations of the previous sections, $\epsilon = h$ so that a Jeans-mass clump will collapse; however, because both gravity and pressure forces between particles within the volume of a kernel are reduced in magnitude, it collapses *more slowly* than it should.

This artificially slow collapse of a Jeans-mass clump is the source of the problem in the 1.0×10^4 particle test calculation. Let us consider what resolution is required to follow correctly the evolution of the elongated structure that is formed at $t \approx 1.12 t_{\rm ff}$. The criterion to be satisfied is that the

© Royal Astronomical Society • Provided by the NASA Astrophysics Data System

Downloaded from https://academic.oup.com/mnras/article/288/4/1060/974629 by guest on 20 August 2022

1997MNRAS.288.1060B

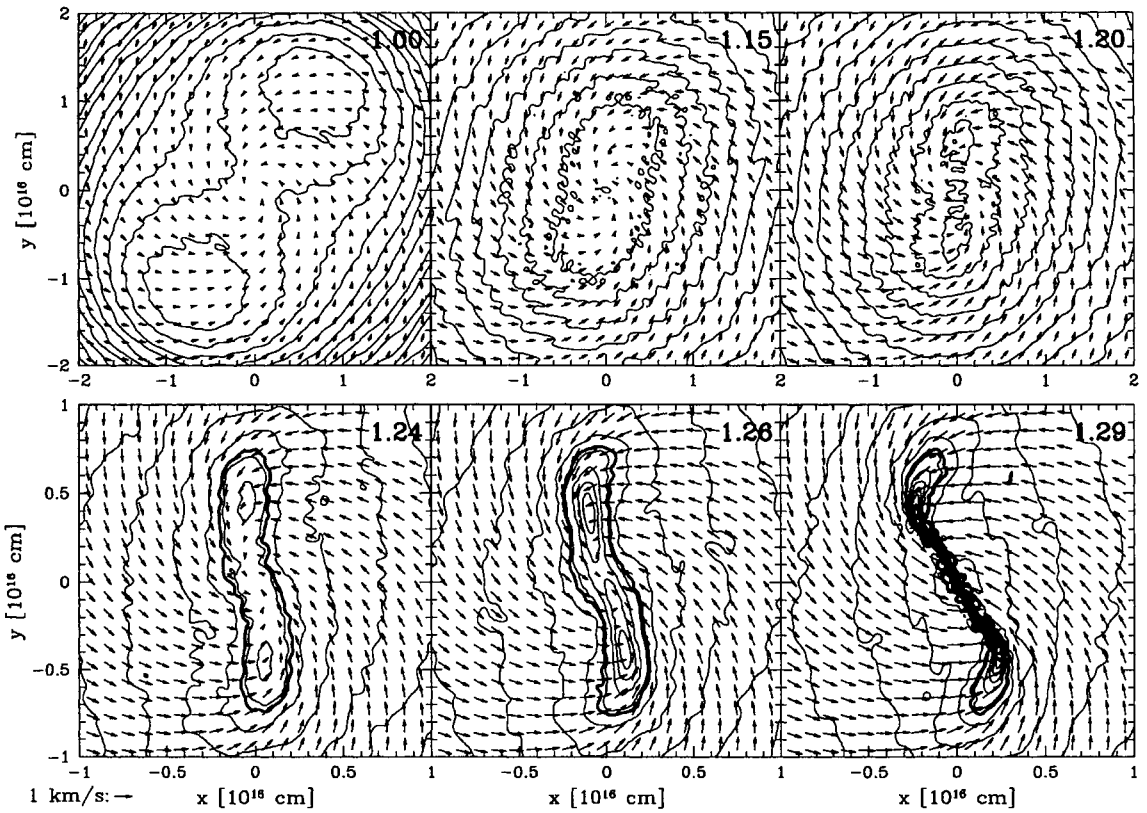

Figure 7. Density and velocity in the x–y plane for the binary-bar fragmentation test calculation performed with SPH using 2.0×10^4 particles. See Fig. 4 for details.

minimum resolvable mass must always be less than a Jeans mass. The Jeans mass is given by Tohline (1982) as

$$M_{\rm J} = \left(\frac{5R_{\rm g}T}{2G\mu}\right)^{3/2}\left(\frac{4}{3}\pi\rho\right)^{-1/2}, \tag{5}$$

where T is the temperature, μ is the mean molecular weight, $R_{\rm g}$ is the gas constant, and G is the gravitational constant. As described above, we take the minimum resolvable mass in an SPH calculation to be the mass of $2N_{\rm neigh}$ particles. Assuming that all particles have equal mass, this is

$$M_{\rm res} \approx M_{\rm tot}\left(\frac{2N_{\rm neigh}}{N_{\rm tot}}\right), \tag{6}$$

where $M_{\rm tot}$ and $N_{\rm tot}$ are the total mass and number of particles, respectively. Combining equations (5) and (6) gives the maximum resolvable density for an SPH collapse calculation,

$$\rho_{\rm crit} \approx \left(\frac{3}{4\pi}\right)\left(\frac{5R_{\rm g}T}{2G\mu}\right)^3\left(\frac{N_{\rm tot}}{2N_{\rm neigh}}\,\frac{1}{M_{\rm tot}}\right)^2. \tag{7}$$

For the current test calculation, with $N_{\rm neigh} = 50$, this critical density is $\rho_{\rm crit} \approx 7 \times 10^{-24}(N_{\rm tot})^2$. Fig. 5 compares the critical density with the maximum density during each test calculation. It can be seen that with 1.0×10^4 particles, $\rho_{\rm crit}$ is reached soon after the two overdense regions merge to form the elongated structure ($t \approx 1.15\,t_{\rm ff}$) and before the expected formation of the binary. With greater numbers of particles, $\rho_{\rm crit}$ is reached only after the elongated structure grows in mass via accretion and each end begins to collapse to higher densities ($t \approx 1.20\,t_{\rm ff}$). In particular, with 2.0×10^4 particles, $\rho_{\rm crit}$ is only barely high enough for the accretion on to the elongated structure and its subsequent collapse into two fragments to be followed correctly. This confirms our choice of the mass of $\approx 2N_{\rm neigh}$ particles as the minimum resolvable mass.

With $\epsilon = h$, if the above density criterion is adhered to, then fragmentation is correctly calculated. If it is not, fragmentation is inhibited. Regions of high density with greater than a Jeans mass collapse too slowly, and hence may unphysically merge with other regions (as in this calculation) or be tidally disrupted before they can collapse.

Since the cause of this problem is the softening of gravity forces on a scale less than $\epsilon = h$, one might consider using $\epsilon < h$. However, as shown in Section 3, this leads to pressure forces between particles being reduced faster than the gravitational force between them which can result in *artificially induced* collapse and, potentially, fragmentation on a scale less than the formal resolution of SPH! To demonstrate this, we present the results from the test case performed with 1.0×10^4 particles, but using a constant gravitational softening length of $\epsilon = 1.0 \times 10^{14}$ cm rather than $\epsilon = h$ (Fig. 8). Indeed, the collapse of each end of the elongated structure to form a fragment is not inhibited (see the growth of maximum density versus time in Fig. 5 and the density contours in Fig. 8 at $t = 1.20\,t_{\rm ff}$). However, at $t = 1.24\,t_{\rm ff}$, *each* end

© Royal Astronomical Society • Provided by the NASA Astrophysics Data System

Downloaded from https://academic.oup.com/mnras/article/288/4/1060/974629 by guest on 20 August 2022

1997MNRAS.288.1060B

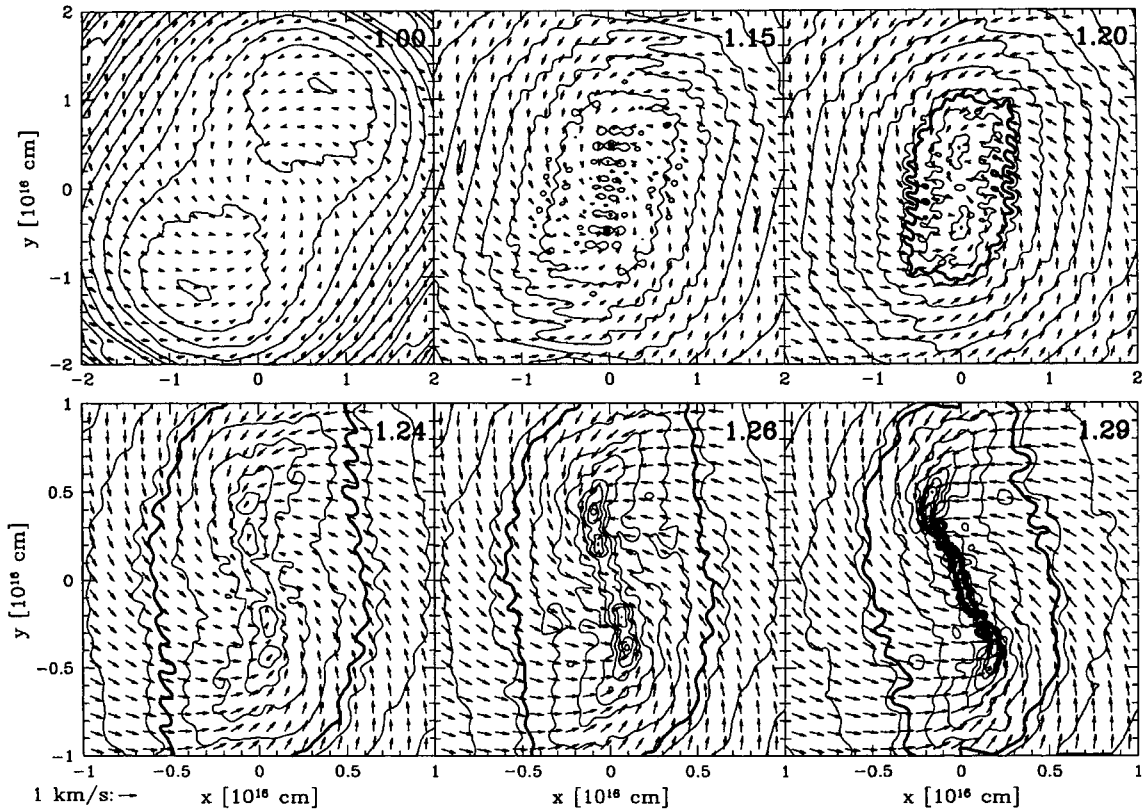

Figure 8. Density and velocity in the x–y plane for the binary-bar fragmentation test calculation performed with SPH using 1.0×10^4 particles, but with $\epsilon = 2.0 \times 10^{14}$ cm rather than $\epsilon = h$ as in Fig. 6. See Fig. 4 for details.

of the elongated structure collapses to form two individual fragments. At $t = 1.29\, t_{\rm ff}$, this results in four fragments with a bar of gas between them. This incorrect fragmentation results from the pressure forces between particles being smoothed faster than the gravitational forces; the lack of pressure support allows each collapsing fragment to hierarchically fragment. With 2.0×10^4 particles and $\epsilon < h$, this artificial fragmentation still occurs, although each pair of fragments quickly merges. With higher resolution, the artificial fragmentation does not occur, because each Jeans mass contains several smoothing kernels, and thus the mass contained within each kernel is sufficiently below a Jeans mass.

In short, the resolution of the code is given by the larger of the smoothing length h and the softening length ϵ; attempting to improve on this resolution by ad hoc methods solves one problem while creating another. Fragmentation is inhibited when the softening of gravity is performed with $\epsilon \gtrsim h$, while with $\epsilon < h$ fragmentation may be artificially induced. If possible, SPH should be implemented so as to maintain $\epsilon = h$, since then artificial fragmentation is inhibited, and the hydrodynamic and gravitational resolutions are equal. If this is not possible, for example, because the SPH code is implemented using the GRAPE hardware, then the gravitational softening length ϵ should be made equal to the smoothing length h that the gas particles have when the density is equal to $\rho_{\rm crit}$. This will stop the artificial fragmentation that can be induced when $\epsilon < h$ and the mass contained within a kernel is close to a Jeans mass. Finally, SPH should not be implemented so that $\epsilon > h$ before $\rho_{\rm crit}$ is reached, since in this case the gravitational resolution limit of the code is reached before the hydrodynamic resolution limit is reached. If the gravitational resolution of the code is lower than the hydrodynamic resolution, then the calculations may become unphysical when the Jeans length is less than $\approx 2\epsilon$, because Jeans-mass clumps will be stabilized against collapse.

A collapse calculation that obeys the above criterion should strictly be halted as soon as $\rho > \rho_{\rm crit}$, because, after this point, the results may depart from reality. However, this criterion alone is too stringent if $\rho_{\rm crit}$ is reached only within an already condensed fragment. If the global result does not depend on the internal evolution of the fragments, the calculation will give the correct global evolution long after $\rho_{\rm crit}$ is passed. Indeed, this assumption was used by Bate et al. (1995) to allow fragments to be replaced by 'sink' particles in order to reduce the computation time for fragmentation calculations. For example, with 2.0×10^4 particles the binary fragmentation and self-gravitating bar are in qualitative agreement with the grid-code, even though the maximum density passes $\rho_{\rm crit}$ only shortly after the binary fragments begin to form. Also, when the 'standard isothermal test case' (Boss & Bodenheimer 1979) was computed by Bate et al. (1995) using SPH, only 8.0×10^3 particles were used, but the calculation gave excellent agreement with the grid-code results of Myhill & Boss (1993) well after the above criterion was broken. These calculations give good agreement long after $\rho_{\rm crit}$ is surpassed, because only the small regions

© Royal Astronomical Society • Provided by the NASA Astrophysics Data System

Downloaded from https://academic.oup.com/mnras/article/288/4/1060/974629 by guest on 20 August 2022

1997MNRAS.288.1060B

within the fragments themselves are incorrectly modelled. Thus, rather than monitoring just the *maximum* density in an SPH calculation, the *locations* where the density exceeds the critical density should be considered.

The heavy contour lines in Figs 4, 6, 7 and 8 show the regions within which $\rho > \rho_{\rm crit}$ (in Fig. 4 the heavy contours are deep within the fragments). With 1.0×10^4 particles, the affected region is most of the centre of the cloud after $t \approx 1.16\, t_{\rm ff}$ (Fig. 6). Thus the fragmentation calculation becomes unreliable beyond this point. With 3.0×10^4 particles and higher, the Jeans-mass criterion is broken only within the fragments (e.g. Fig. 4). Therefore, until the dense bar of gas forms between the binary, only the evolution inside the fragments may be handled incorrectly. The calculation with 2.0×10^4 particles (Fig. 7) is an intermediate case; the region where $\rho > \rho_{\rm crit}$ includes both fragments and the gas between them, and yet the binary fragmentation is just resolved.

Finally, even if $\rho > \rho_{\rm crit}$ for a finite region of a simulation, the results in this region are not necessarily incorrect. If it is impossible for this region to gather a Jeans mass, then breaking the resolution criterion will not matter. For example, if the gas with $\rho > \rho_{\rm crit}$ falls on to a fragment faster than it can collapse under its self-gravity, further fragmentation will be prevented. Considering the velocity of the gas within the regions with $\rho > \rho_{\rm crit}$ in the 8.0×10^4 particle calculation, we find that, indeed, the gas falls to the centre of the fragments faster than it can collapse under its own self-gravity up until $t \approx 1.28\, t_{\rm ff}$. Thus the calculation can be correctly followed to this point. Beyond this, the bar between the binary has a density $\rho > \rho_{\rm crit}$, and the velocity along the bar is low. Thus we cannot determine the correct evolution of the bar. A similar problem occurs if, rather than being in free-fall on to a fragment, the gas becomes rotationally supported around a fragment and its density is greater than $\rho_{\rm crit}$. In this case, fragmentation of the disc will be inhibited (if $\epsilon \geq h$), or may be artificially induced (if $\epsilon < h$).

8 BAR FRAGMENTATION

When Burkert & Bodenheimer (1993) first presented their fragmentation calculation, they found that after the fragmentation to form a binary, a self-gravitating bar of gas formed between the binary and fragmented. This formation and fragmentation of a high-density bar between two fragments is not unique; other initial conditions also lead to this state (e.g. Bonnell et al. 1991). In the calculation of Burkert & Bodenheimer (1993) the bar fragmented into nine fragments. In Section 5, using the same code but with the inclusion of an artificial viscosity and heating to keep the local Jeans length larger than the zone size, six fragments form inside the bar, with two additional fragments in the discs around the binary components. The number of fragments produced from the bar fragmentation depends on the resolution. With higher resolution, the collapse of the bar is halted, due to artificial viscosity and heating, when the bar is thinner, and more fragments will be produced because the ratio of the length of the bar to its width is larger. In the calculation presented here, the bar is constrained to be ≈ 3 grid cells in thickness by the artificial viscosity and heating. With unlimited resolution and without heating, the bar may collapse to an infinite-density filament, as suggested by the work of Inutsuka & Miyama (1992) and by Truelove et al. (1997).

Similarly, with SPH, we cannot determine what the result is with a purely isothermal equation of state. With 8.0×10^4 particles, the calculation can be followed correctly up to densities of $\rho_{\rm crit} \approx 10^{-13}$ g cm^{-3}. Beyond this density, a Jeans mass is composed of less than $\approx 2N_{\rm neigh}$ particles and is not correctly resolved. However, in reality, the gas should become optically thick at around this density and start to heat with a polytropic constant $\gamma = 7/5$ (Tohline 1982). This fact can be exploited to allow the calculation to be followed further than with a purely isothermal equation of state, since the Jeans mass will increase with increasing density, rather than decrease, and thus the Jeans mass can always be kept above the mass of $\approx 2N_{\rm neigh}$ particles.

In the following calculations, we use the polytropic equation of state

$$P = K\rho^{\gamma}, \tag{8}$$

where K is a constant that is set equal to the square of the isothermal sound speed $c_{\rm s}$. The polytropic constant γ varies with density as

$$\begin{aligned} &\gamma = 1, && \rho \leq \tau \times 10^{-13} \text{ g cm}^{-3}, \\ &\gamma = 7/5, && \tau \times 10^{-13} < \rho \leq 10^{-11} \text{ g cm}^{-3}, \\ &\gamma = 5/3, && \rho > 10^{-11} \text{ g cm}^{-3}, \end{aligned} \tag{9}$$

and τ controls the density at which the heating starts due to the gas becoming optically thick. The change of γ from 7/5 to 5/3 is used, instead of a minimum smoothing length, to stop the contraction of high-density fragments and, thus, to keep the time-steps large enough to continue the calculation. No minimum smoothing length is enforced. With $\tau \lesssim 1$, this equation of state allows us to follow the calculation indefinitely, since the mass of $2N_{\rm neigh}$ particles is always less than a Jeans mass. Compared to maintaining a purely isothermal equation of state, heating the gas provides extra support against the collapse of the bar upon itself. Beginning the heating at a lower density more strongly inhibits fragmentation of the bar, because the Jeans mass is increased. Thus, if the bar fragments with a certain value of τ, then more fragments are likely to be produced with less heating (assuming that collapse to an infinite-density filament is avoided).

In Fig. 9, we follow the fragmentation calculation until $t = 1.315\, t_{\rm ff}$ with $\epsilon = h$ and using the polytropic equation of state with $\tau = 1$. After the fragmentation to form a binary, a bar of gas forms between them, as in the previous calculations. The bar grows in density, becomes self-gravitating, and fragments at $t = 1.31\, t_{\rm ff}$ when the density in the bar is $\approx 10^{-12}$ g cm^{-3}. Since a Jeans mass is always resolved, the fragmentation is not a numerical effect, although the *positions* of fragments along the bar do depend on numerical noise. Four fragments are formed in the fragmenting bar. Also, just before the bar fragments, a disc fragmentation occurs in the circumstellar disc surrounding one of the original binary fragments; although the initial conditions were symmetric, numerical noise has grown throughout the calculation which leads to symmetry breaking. In total, five fragments form in addition to the original binary. Two more calculations, with the heating beginning at lower densities ($\tau = 0.1$ and 0.3), were also performed. With $\tau = 0.3$, a single

Downloaded from https://academic.oup.com/mnras/article/288/4/1060/974629 by guest on 20 August 2022

© Royal Astronomical Society • Provided by the NASA Astrophysics Data System

1997MNRAS.288.1060B

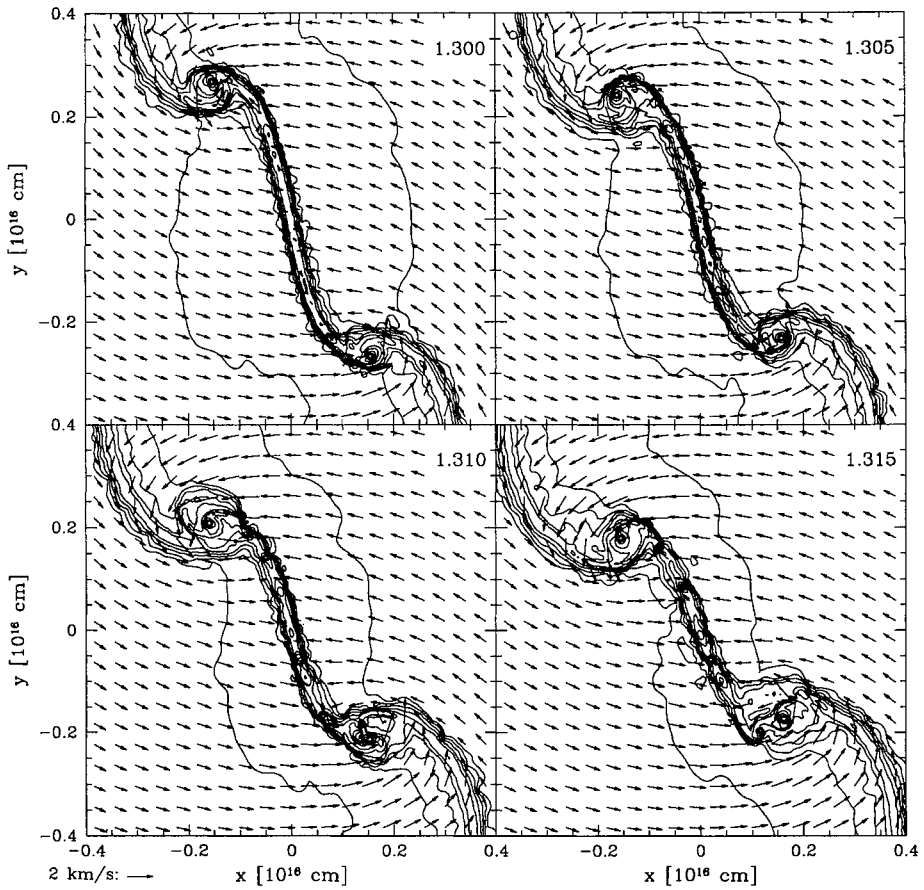

Figure 9. Density and velocity in the x–y plane for the binary-bar fragmentation test calculation performed with SPH using 8.0×10^4 particles, a polytropic equation of state, and $\epsilon = h$. Density contours are drawn every 1/2 of a decade. Velocity vectors are given with length proportional to speed; an arrow representing 2 km s^{-1} is given beneath the frames. Times are given for each frame in units of the initial cloud free-fall time $t_{\rm ff} = 1.0774 \times 10^{12}$ s.

fragment was formed near the centre of the bar, and neither of the circumstellar discs fragmented. With $\tau = 0.1$, no fragments were formed apart from the original binary; the gas in the self-gravitating bar was slowly accreted by the two protostars.

Therefore, whether or not the bar fragments depends sensitively on when the gas becomes optically thick and starts to heat. For the above equation of state, the bar will fragment only if $\tau \gtrsim 0.3$, with the number of the fragments increasing as τ is increased. If fragments are formed in the bar, they subsequently fall towards the closest of the original fragments (as does the gas in the bar with $\tau = 0.1$). Their survival or merger depends on chaotic interactions and the sizes of the protostellar fragments. For example, in the calculation of Fig. 9, one of the fragments from the bar merges with the fragment produced via the disc fragmentation.

9 CONCLUSIONS

We have determined what resolution is required for a smoothed particles hydrodynamics (SPH) code with self-gravity to follow collapse and fragmentation problems correctly. If the required resolution is not used, the fragmentation may be incorrectly modelled, with the results depending on the method by which the gravitational and pressure forces between particles are softened and smoothed, respectively. If the scale for softening the gravitational forces ϵ is greater than or equal to the hydrodynamic smoothing length h, then collapse and/or fragmentation of Jeans-mass clumps on the scale of h is inhibited. If gravity is softened on a shorter scale than h, then collapse and/or fragmentation of a near-Jeans-mass clump may be artificially induced. These problems may manifest themselves in any SPH calculations which include self-gravity (e.g., cosmological-structure and galaxy formation calculations).

To avoid these resolution problems, an SPH calculation must obey the resolution criterion that the minimum resolvable mass is always less than the local Jeans mass. In practice, this means that, if the code is implemented such that $\epsilon = h$, the minimum Jeans mass that is reached during the calculation must always be greater than approximately twice the number of particles in an SPH kernel ($2N_{\rm neigh}$). If a fixed value of ϵ must be used to implement the SPH code, then ϵ should be chosen to be equal to the value that h has when the mass of $2N_{\rm neigh}$ particles is equal to the Jeans mass. An SPH code should not be implemented with $\epsilon > h$, since then the gravitational resolution is lower than the hydrodynamic resolution. If this criterion is obeyed, the dependence of the results on the method by which the smoothing and softening are done is avoided.

© Royal Astronomical Society • Provided by the NASA Astrophysics Data System

Downloaded from https://academic.oup.com/mnras/article/288/4/1060/974629 by guest on 20 August 2022

1997MNRAS.288.1060B

As an example of the importance of this criterion, we have presented calculations of a demanding fragmentation calculation performed with an Eulerian grid code and with SPH. We find that the SPH results are in good qualitative and quantitative agreement with those from the Eulerian grid code, provided that this resolution criterion is adhered to.

Finally, we note that the need for this criterion is unrelated to the need for the Jeans constraint suggested by Truelove et al. (1997). They require the minimum resolvable mass to be less than the local Jeans mass to avoid the growth of numerical perturbations, whereas the criterion presented here is required so that the behaviour of near-Jeans-mass clumps is determined by physical processes and not on the specific implementation of the SPH code. However, in both cases the minimum resolvable mass is required to be always less than the Jeans mass and, thus, in satisfying one of these constraints the other is also satisfied.

ACKNOWLEDGMENTS

We are grateful to Ian Bonnell and Peter Bodenheimer for many helpful discussions, and to Ian Bonnell and Matthias Steinmetz for critically reading the manuscript.

REFERENCES

Bate M. R., Bonnell I. A., Price N. M., 1995, MNRAS, 277, 362
Benz W., 1990, in Buchler J. R., ed., The Numerical Modeling of Nonlinear Stellar Pulsations: Problems and Prospects. Kluwer, Dordrecht, p. 269
Benz W., Bowers R. L., Cameron A. G. W., Press W., 1990, ApJ, 348, 647
Bodenheimer P., Boss A. P., 1981, MNRAS, 197, 477
Bonnell I., Martel H., Bastein P., Arcoragi J.-P., Benz W., 1991, ApJ, 377, 553
Boss A. P., Bodenheimer P., 1979, ApJ, 234, 289
Burkert A., Bodenheimer P., 1993, MNRAS, 264, 798
Burkert A., Bodenheimer P., 1996, MNRAS, 280, 1190
Burkert A., Bate M. R., Bodenheimer P., 1997, MNRAS, in press
Davies M. B., Ruffert M., Benz W., Müller E., 1993, A&A, 272, 430
Durisen R. H., Gingold R. A., Tohline J. E., Boss A. P., 1986, ApJ, 305, 281
Evrard A. E., 1988, MNRAS, 235, 911
Gingold R. A., Monaghan J. J., 1977, MNRAS, 181, 375
Gingold R. A., Monaghan J. J., 1981, MNRAS, 197, 461
Gingold R. A., Monaghan J. J., 1982, MNRAS, 199, 115
Hernquist L., Katz N., 1989, ApJS, 70, 419
Inutsuka S., Miyama S. M., 1992, ApJ, 388, 392
Lucy L., 1977, AJ, 82, 1013
Monaghan J. J., 1992, ARA&A, 30, 543
Monaghan J. J., Gingold R. A., 1983, J. Comput. Phys., 52, 374
Monaghan J. J., Lattanzio J. C., 1985, A&A, 149, 135
Monaghan J. J., Lattanzio J. C., 1986, A&A, 158, 207
Myhill E. A., Boss A. P., 1993, ApJS, 89, 345
Navarro J. F., White S. D. M., 1993, MNRAS, 265, 271
Owen J. M., Villumsen J. V., 1997, ApJ, in press
Sommer-Larsen J., Vedel H., Hellsten U., 1997, ApJ, submitted
Steinmetz M., 1996, MNRAS, 278, 1005
Steinmetz M., Müller E., 1993, A&A, 268, 391
Tohline J. E., 1982, Fundam. Cosmic. Phys., 8, 1
Truelove J. K., Klein R. I., McKee C. F., Holliman J. H., Howell L. H., Greenough J. A., 1997, ApJ, submitted
von Neumann J., Richtmyer R. D., 1950, J. Appl. Phys., 21, 232
Woodward P. R., Colella P., 1984, J. Comput. Phys., 54, 115

Downloaded from https://academic.oup.com/mnras/article/288/4/1060/974629 by guest on 20 August 2022

© Royal Astronomical Society • Provided by the NASA Astrophysics Data System